EASR

Engineering and Applied Science Research

https://www.tci-thaijo.org/index.php/easr/index

Published by the Faculty of Engineering, Khon Kaen University, Thailand

Influence of laminar and turbulent flow on signal response of gas sensors in electronic nose chamber for detecting rancid odor in brown rice (cv. Khao Dawk Mali 105)

Phongprapan Kantakaew*[1, 2)], Damorn Bundhurat[1)], Viboon Changrue[1)] and Natawut Neamsorn[1, 2)]

[1)]Department of Mechanical Engineering, Faculty of Engineering, Chiang Mai University, Chiang Mai 50200, Thailand
[2)]Postharvest Technology Innovation Center, Office of the Higher Education Commission, Bangkok 10400, Thailand

Received 2 August 2023
Revised 16 January 2024
Accepted 18 January 2024

Abstract

The aim of this research was to investigate the influence of flow pattern of the gas carrier inside the electronic nose chamber on the response rate of the signal from an array of gas sensors. The gas sensors in the electronic nose chamber were tested with laminar flow and turbulent flow. The principles of Reynolds number and the Navier-Stokes equation were employed to calculate and model the airflow in Computational Fluid Dynamics (CFD) simulations. The simulated airflow was compared to the actual airflow using smoke as a visual indicator to indicate the type of flow. Variables and conditions derived from the flow patterns were used in an actual experiment of electronic nose to detect specific odor compounds in brown rice (cv. KDML105). The six sensors were installed in an electronic nose chamber. The signals from the experiment were then used to determine the most effective sensor response between laminar and turbulent flow. Significantly different results were observed between the two flow patterns with a p-value < 0.05 for five out of six sensors. Additionally, the analysis of the rate of signal change indicated that the laminar flow pattern had higher values compared to the turbulent flow pattern.

Keywords: Electronic nose, Flow pattern, Gas carrier, Rancid odor

1. Introduction

The electronic nose (e-nose) was created to simulate human olfaction and is a measuring and sensing tool that uses an array of gas sensors and signal processing algorithms, as well as pattern recognition techniques, to identify and measure odors. The sensors used in measurement may be various types of polymer sensors or metal oxide semiconductors (MOS) with a carrier gas to pass the odor or chemical substance through the sensors. In recent decades, e-noses have gained significant international attention and can be used to detect and identify various odors and volatile organic compounds. It is an important tool for non-destructive testing, especially in the food and agriculture industries [1]. One of the important advantages of using e-noses is their ability to detect subtle changes in odors or volatile compounds, which can indicate changes in the quality, ripeness, or freshness of agricultural products [2]) For example, e-noses can detect changes in the smell of fruits and vegetables during the ripening process, allowing producers to harvest them at the optimal time so as to increase quality and prolong shelf life [3]. Other than their use in food and agriculture, e-nose are widely used in various industries, such as healthcare [4], environmental monitoring [5], disease diagnosis [6], air quality assessment [7], and identifying product defects [8]. E-noses can also be used to detect contaminants and adulterants in food products, such as easy-to-volatile organic compounds (VOCs), which may indicate the presence of pollutants such as insecticides, herbicides, or fungicides. Another advantage of the e-nose is that the testing process is quick and does not destroy or alter the sample in any way, making it possible to test large quantities of products quickly and efficiently at a reasonable cost [9]. When molecules from the substance pass through the sensor, they accumulate on the surface, causing the sensor to expand, resulting in a physical change. This leads to a change in electrical conductivity[10].

Gas carriers or gases for transporting odors to e-nose sensors are considered important components of the e-nose system, as they help transport odor samples from the source or storage container to the sensor in the e-nose chamber [11]). However, gas carriers have some limitations that may affect the accuracy and reliability of e-nose measurements, such as they can dilute the odor sample, resulting in a decrease in the concentration of volatile compounds, which can make it more difficult for the e-nose sensor to detect and identify specific odors or volatile compounds. This can affect the sensitivity and responsiveness of e-nose sensors, particularly if the concentration is low [12]. Currently, e-noses are being applied to classify rancid odors in brown rice cv. KDML 105 [13]. This attracted researchers to conduct in-depth studies related to the gas flow patterns that carry the sample gas into the e-nose chamber, using engineering calculations techniques. The study investigates the flow of the gas in the e-nose system, utilizing the principles of Reynold number and Navier-Stokes equation to define two flow patterns: (1) laminar flow and (2) turbulent flow. The aim is to compare the gas flow patterns that result in the most efficient response from the e-nose sensors in terms of their sensitivity.

*Corresponding author.
Email address: Phongprapan_ka@cmu.ac.th
doi: 10.14456/easr.2024.22

2. Materials and methods

2.1 Computational fluid dynamics analysis

The experimental verification is conducted using CFD in the e-nose system. The calculation of the computational results in this research aims to emphasize the comparison with the results of the actual experimental airflow patterns in an electronics chamber, using the ANSYS 2020 R1 software. There are two flow patterns, the first being a laminar flow pattern, which utilizes the principles of the Reynolds number (1)

$$Re = \frac{\rho u_{in} D_{in}}{\mu} \tag{1}$$

where u_{in} is the average velocity at the inlet, D_{in} is the inlet diameter, ρ is the fluid density and μ is dynamic viscosity and the Navier-Stokes equations, which form a system of partial differential equations. This system includes continuity equation (2), the conservation of mass equation (3), and the component mass conservation equation (4). These equations are employed to generate an efficient airflow pattern of the gas carrier in the e-nose system.

$$\frac{\partial u_i^*}{\partial x_i^*} = 0 \tag{2}$$

$$\frac{\partial(\rho u)}{\partial x} + \frac{\partial(\rho v)}{\partial y} + \frac{\partial(\rho w)}{\partial z} = 0 \tag{3}$$

$$\frac{\partial(\rho c_s)}{\partial t} + \vec{\nabla} \cdot (\rho u_i c_s) = \vec{\nabla} \cdot \left(D_s \cdot \nabla(\rho c_s)\right) + S_s \tag{4}$$

where x_i^* is the position vector, u_i^* is the velocity vector, t is the time, u, v, and w are the components of the velocity vector in the x, y, and z directions, respectively, c_s is the volume concentration of component s, ρc_s is the mass concentration of component, D_s is the diffusion coefficient of the component, and S_s is the mass of component produced by the chemical reaction per unit volume in unit time.

Setting boundary conditions on the parser uses Fluent in the ANSYS component. The Reynolds number obtained in the calculation of e-nose chamber model was less than 2300, so the numerical simulation process was a laminar flow process [14]. The boundary conditions for simulating the flow field are shown in Table 1.

Table 1 The boundary conditions for simulating the flow field of a laminar flow pattern.

Parameters	**Values**
Simulated state	Steady state
Model	Laminar
Air density (kg m^{-3})	1.225
Dynamic Viscosity (Pa·s)	1.8277×10^{-5}
Pressure (Pa)	101.3×10^3

The next flow pattern is the turbulent flow pattern, which consists of equations similar to the laminar flow pattern. However, due to the different nature of the flow, the motion equations of turbulent flow are more complex. In this research, the standard k-epsilon turbulence model [15] is chosen as the preferred modeling equation, which is well-known and widely used. It consists of the turbulent kinetic energy equation (5) and the turbulence dissipation rate equation (6), as shown below:

$$\frac{\partial \rho k}{\partial t} = \frac{\partial}{\partial x_k}\left[\frac{\mu_t}{\sigma_k}\frac{\partial k}{\partial x_k}\right] + \mu_t\left(\frac{\partial U_i}{\partial x_k} + \frac{\partial U_k}{\partial x_i}\right)\frac{\partial U_i}{\partial x_k} - \rho\varepsilon \tag{5}$$

$$\frac{\partial \rho \varepsilon}{\partial t} = \frac{\partial}{\partial x_k}\left[\frac{\mu_t}{\sigma_\varepsilon}\frac{\partial \varepsilon}{\partial x_k}\right] + \frac{C_1 \mu_t \varepsilon}{k}\left(\frac{\partial U_i}{\partial x_k} + \frac{\partial U_k}{\partial x_i}\right)\frac{\partial U_i}{\partial x_k} - \rho C_2 \frac{\varepsilon^2}{k} \tag{6}$$

where x_i and x_k is the Cartesian space coordinate i and k, respectively, μ_t is the turbulence viscosity, ε is rate of dissipation of turbulence energy, k is the turbulence kinetic energy, U_i and U_k is the mean component of velocity in direction i and k, respectively, σ_ε and σ_k is the effective turbulent Prandtl number for transport of ε and k, respectively, and C_1 and C_2 are the coefficients in approximated turbulent transport equations. In setting the boundary conditions for the inlet and outlet of the parallel channel, a periodic flow is assumed during the fully developed flow regime. The calculation will specify equal mass flow rates at both the inlet and outlet [16]. In this study, we used a gas mixture with two types of gases (nitrogen and oxygen) flowing into the chamber. The mass flow controller is used to adjust a mass flow rate and provide continuous gas streams [17]. The selection of oxygen gas as a representative for flow testing is due to its suitability for the sensor group used in the experiments, and its known proportions in the actual air [18].

2.2 Preparation of samples for smoke flow testing

Using Glycol-based compounds, with a volume of 20 ml will be filled into a glass container equipped with a smoke-generating system, with a capacity of approximately 2.5 liters, designed for producing and containing the smoke. This sample will be used to test the flow pattern of the gas in the e-nose system of the e-nose chamber, located in the Agricultural and Food Engineering laboratory at Chiang Mai University. The testing will be conducted at room temperature.

2.3 Preparation of the rancid odor from brown rice

The brown rice is specifically KDML 105 variety, available in Chiang Mai province, Thailand. Take 1 kg of rice with a moisture content of 12% (wet basis). Place it in an open container at room temperature, allowing it to interact with the air, humidity, and sunlight until a rancid odor develops. Then, divide the rice into glass bottles with a capacity of 250 ml each, weighing approximately 50 grams per bottle. Prepare a total of 15 bottles. Let the bottles sit at room temperature for 20 minutes before conducting the tests with the e-nose device.

2.4 Sensors in e-nose chamber

The e-nose chamber is a part of the e-nose device with a box-shaped format measuring 30x30x180 mm^3. It has one gas inlet and one gas outlet (as shown in Figure 1). Inside, there are a total of six gas sensors arranged perpendicular to the gas flow [12]. The gas sensors consist of TGS-813, TGS-822, TGS-2600, TGS-2610, TGS-2611, and TGS-2620 (Figaro Eng., Japan). Each sensor is a metal oxide semiconductor (MOS) type gas sensor with different specific capabilities, and they are organized in an array of gas sensors, as shown in Table 2.

Table 2 Details of sensor.

Sensor	Target Gas	Detection Range
TGS-813	Combustible Gases	500 to 10000ppm
TGS-822	Ethanol and Solvent Vapors	50 to 5000ppm
TGS-2600	Air Contaminants	1 to 100ppm
TGS-2610	LPG	300 to 10000ppm
TGS-2611	Methane (CH_4)	300 to 1000ppm
TGS-2620	Volatile organic compound	50 to 500ppm

The gas sensors in the e-nose chamber are strategically placed in sequential order. TGS-2600, positioned near the gas entrance, has an odor-receiving area of 0.754 mm^2. Following this, TGS-2610, TGS-2611, and TGS-2620, occupying the second, third, and fourth positions, share an odor-receiving area of 11.6 mm^2. In the fifth position is TGS-813, featuring a larger odor-receiving area of 76.2 mm^2. The final sensor, TGS-822, placed near the rear, also boasts a 76.2 mm^2 odor-receiving area. Notably, TGS-813 and TGS-822 share similar external characteristics and larger dimensions than the initial four sensors. The arrangement considers the physical capabilities and odor-receiving areas of each sensor type within the e-nose chamber.

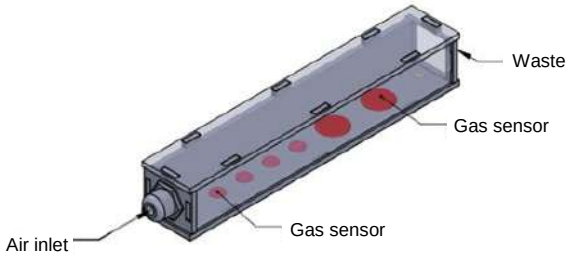

Figure 1 The e-nose chamber.

2.5 Electronic nose system

This e-nose testing apparatus utilizes a micro-pump air delivery system powered by a 5 V direct current. The gas flow rate is controlled by a flow control device which can adjust the flow rate within the range of 0.1 - 0.5 liters per minute. The flow direction is controlled by a solenoid valve that regulates the flow direction of the odor components emitted from the headspace of the sample. There are three solenoid valves, When Valve 2 is opened, it allows the reference gas to flow through and clean the gas sensor chamber, as shown in Figure 2.

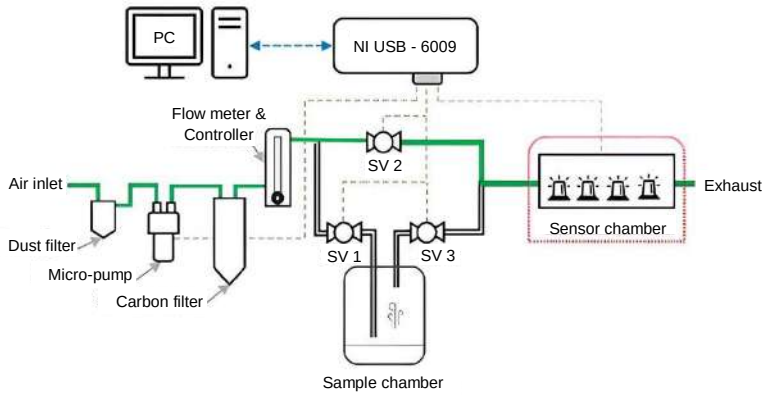

Figure 2 Procedure for cleaning the e-nose system.

When Valve 1 and Valve 3 are opened, the sample gas flows into the gas sensor chamber, as shown in Figure 3. The e-nose apparatus is controlled by a computer through Labview2014 software to read and record the signal results from the gas sensors using an NI USB-6009 signal converter. The experiment will be conducted 45 times, and the data obtained will be further analyzed.

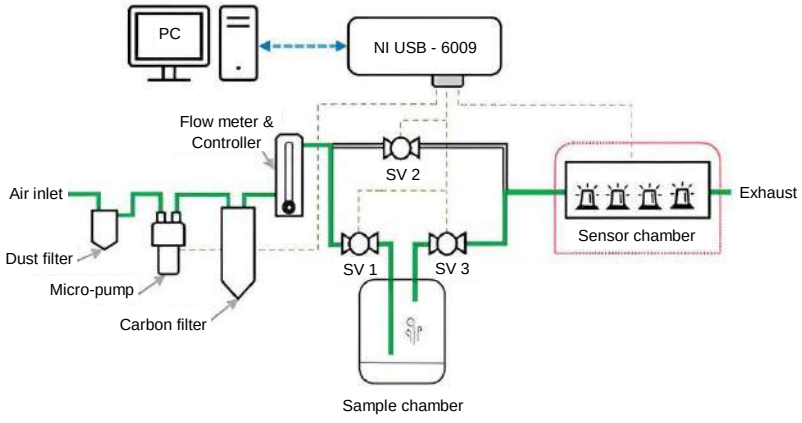

Figure 3 Testing procedures for gas carrier in the e-nose system.

The smoke generator, which is installed in place of the odor sample chamber, is activated to prepare the smoke for testing the airflow pattern in the e-nose system. The gas transportation system of the e-nose operates similarly to the previous odor sample testing process. Specifically, when the air pump is activated, solenoid Valve 1 and solenoid Valve 3 open to allow the transport gas to carry the smoke to the gas sensor chamber. This enables the study of the actual airflow pattern that will occur next (as shown in Figure 3).

2.6 Data analysis

2.6.1 Data collection and feature extraction

In the testing process, the data of the electrical potential difference signals obtained from the gas sensor during the odor testing period are used to generate stable signals that can be later analyzed. The gas odor data from the sample bottle is introduced into the odor transport system for a duration of five minutes. The device then starts separating the gas from the sample bottle, and the gas flows continuously into contact with an array of sensors. This interaction causes a change in the output voltage of the sensors, which ranges from 0 V to 3.3 V. Subsequently, the output voltage is transferred to the computer after undergoing analog-to-digital conversion. As an example of sensor data variations, the data are selected as the sensor response data after passing through 40 seconds to facilitate convenient separation of data features. Figure 4 shows the raw data and various characteristics. The observed fluctuations in the data values are due to the presence of noise signals, as indicated in Figure 4.

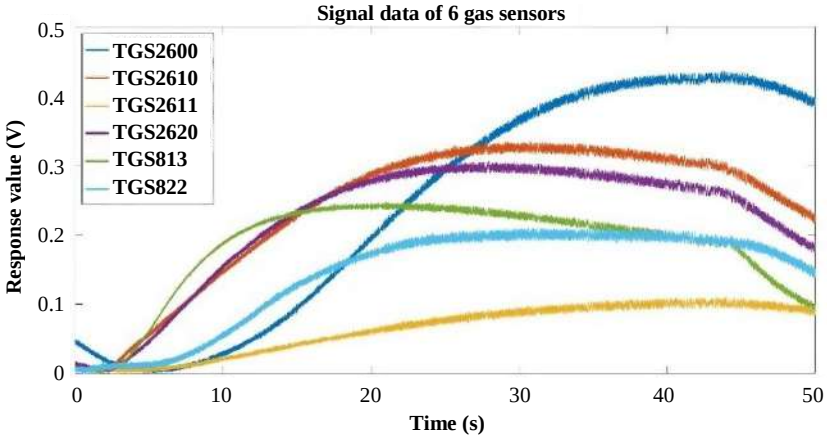

Figure 4 The raw data and various characteristics of six gas sensors.

Preprocessing data before analysis is a highly essential procedure to significantly reduce the physical impact of the measured signals. One commonly used technique for this purpose is the Savitzky-Golay smoothing method, the main feature of which is that, while filtering noise, it can ensure that the shape and width of the signal remain unchanged, which can better retain the information of characteristic peaks and improve the accuracy of input data [19]. Figure 5 provides a visual representation of this process.

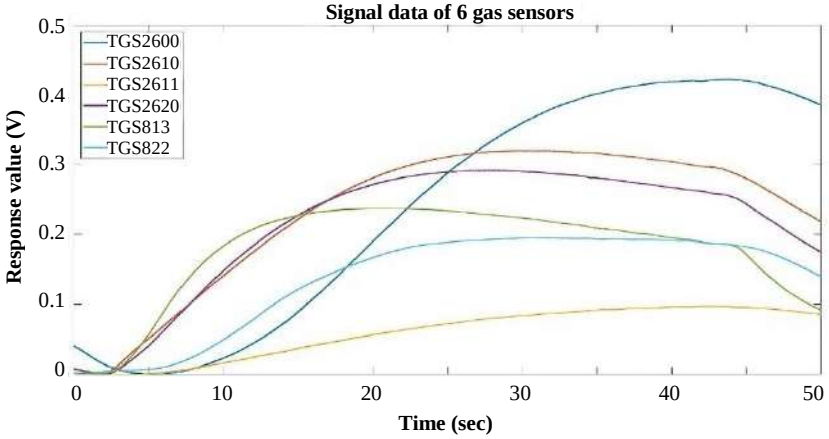

Figure 5 The adjusted data after smoothing method.

3. Results

3.1 Results of creating an airflow model within the e-nose chamber

The flow model in the e-nose chamber was created using ANSYS 2020 R1 software. It used gas with a gas flow rate of 0.4 liter per minute, as shown in Figure 6. The cross-section area of the gas flow expanded as it entered the entrance of the chamber and started to be uniform over the second sensor throughout the exit. A similar pattern was achieved in actual flow using smoke visual test, as seen in Figure 7. The flow started to be uniform over the second sensor and exhibited a laminar pattern. When the average velocity variable values were combined with various properties, it was found that the Reynolds number within the e-nose chamber, characterized by a rectangular shape in the laminar flow model, could be calculated to be 838. However, as the flow approached the position of the last sensor, there was a swirling motion resembling a turbulent flow pattern. This phenomenon may have resulted in the formation of an air wall that caused the airflow to exhibit a turbulent behavior over the last sensor.

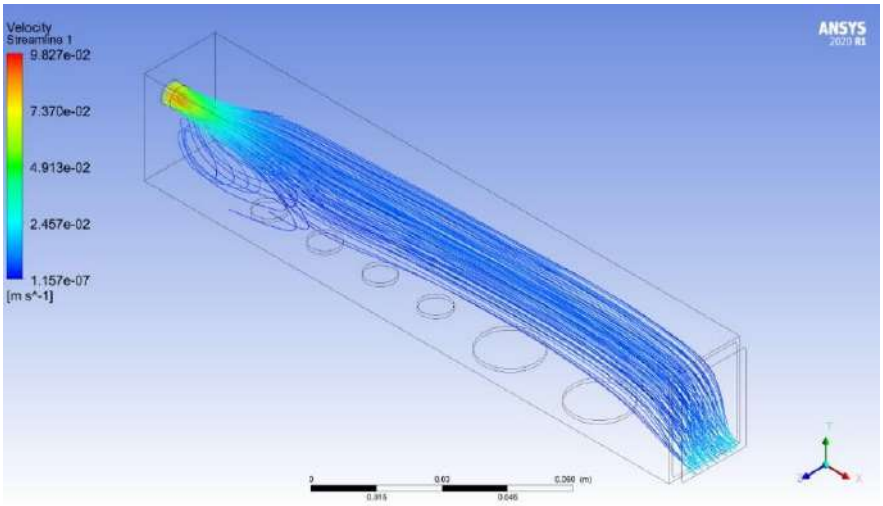

Figure 6 Gas flow model - laminar flow.

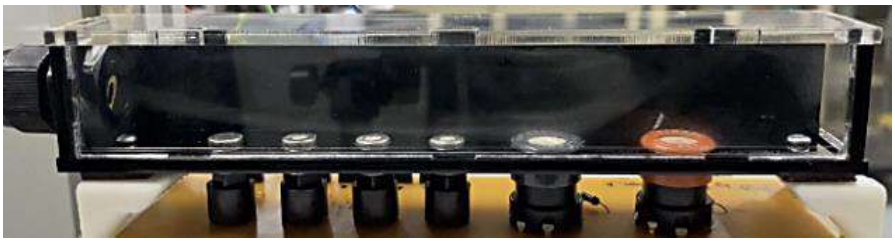

Figure 7 Smoke flow exhibits laminar flow pattern.

The simulation results for the laminar flow pattern of oxygen gas and oxygen mass concentration, with a high flow rate of 0.4 liters per minute at the inlet, are shown in Figures 8 and 9, respectively. In this simulation case, the flow velocity is relatively low, leading to laminar flow. This results in a uniform flow of the gas sample. The velocity vector distribution remains stable over time, as observed in Figure 8. As anticipated, after 50 seconds, the final oxygen concentration field becomes uniform and is distributed over all the gas sensors, as illustrated in Figure 9.

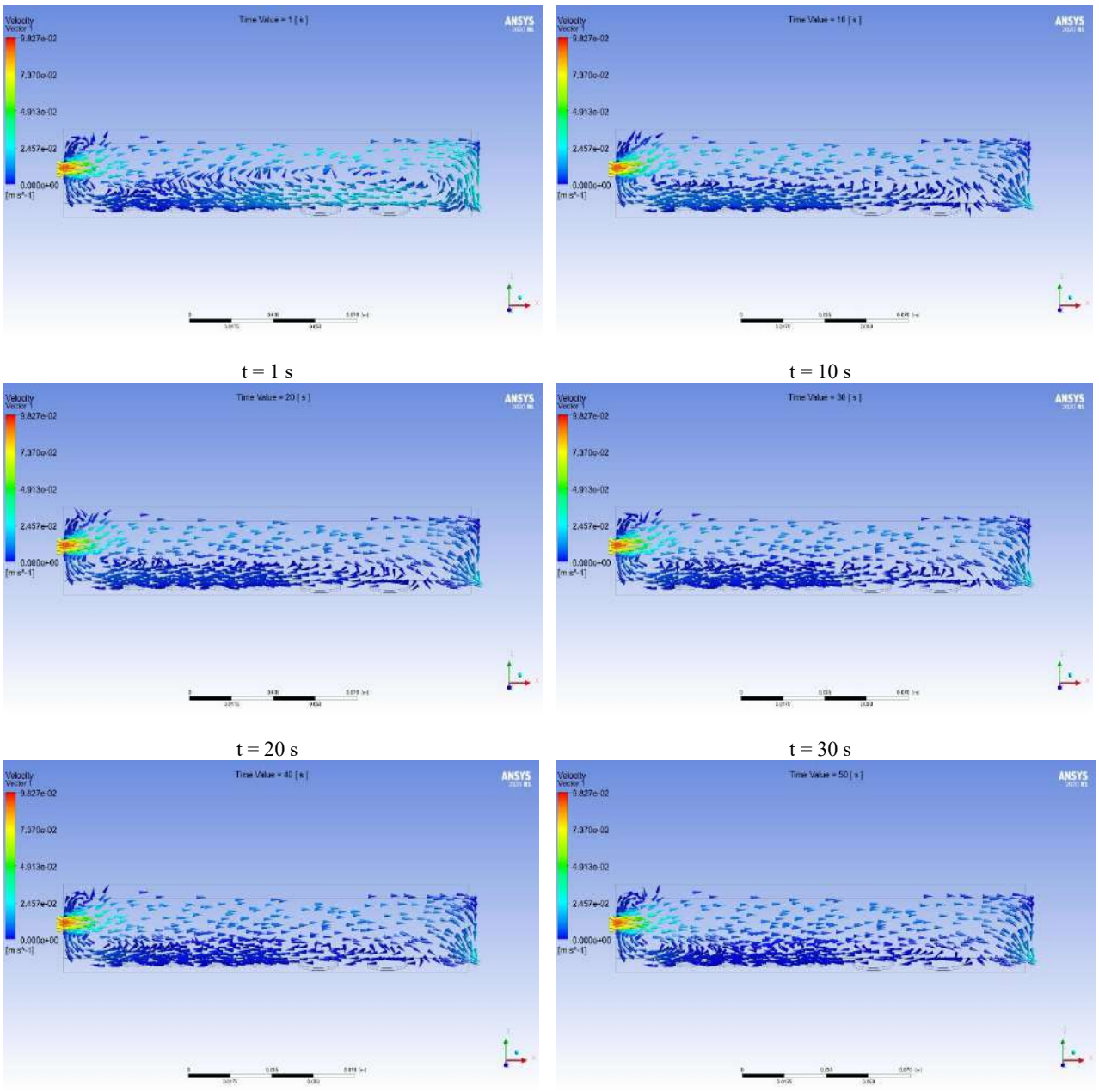

t = 1 s t = 10 s

t = 20 s t = 30 s

t = 40 s t = 50 s

Figure 8 Simulation results on variation of O_2 velocity vector distribution with time at plane XY (z = 10 mm) for the laminar flow pattern.

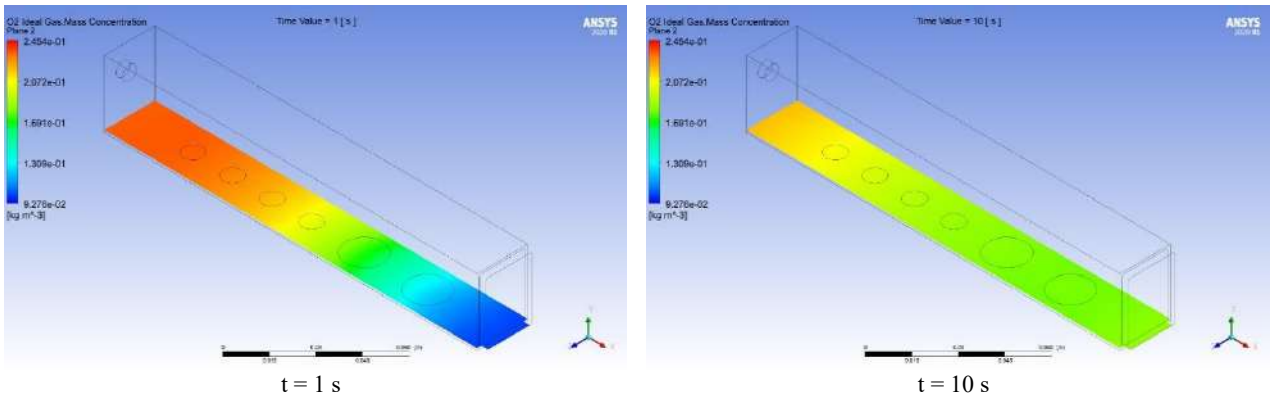

t = 1 s t = 10 s

Figure 9 Simulation results variation of O_2 mass concentrations with time at plane XZ (y = 4 mm) for the laminar flow pattern.

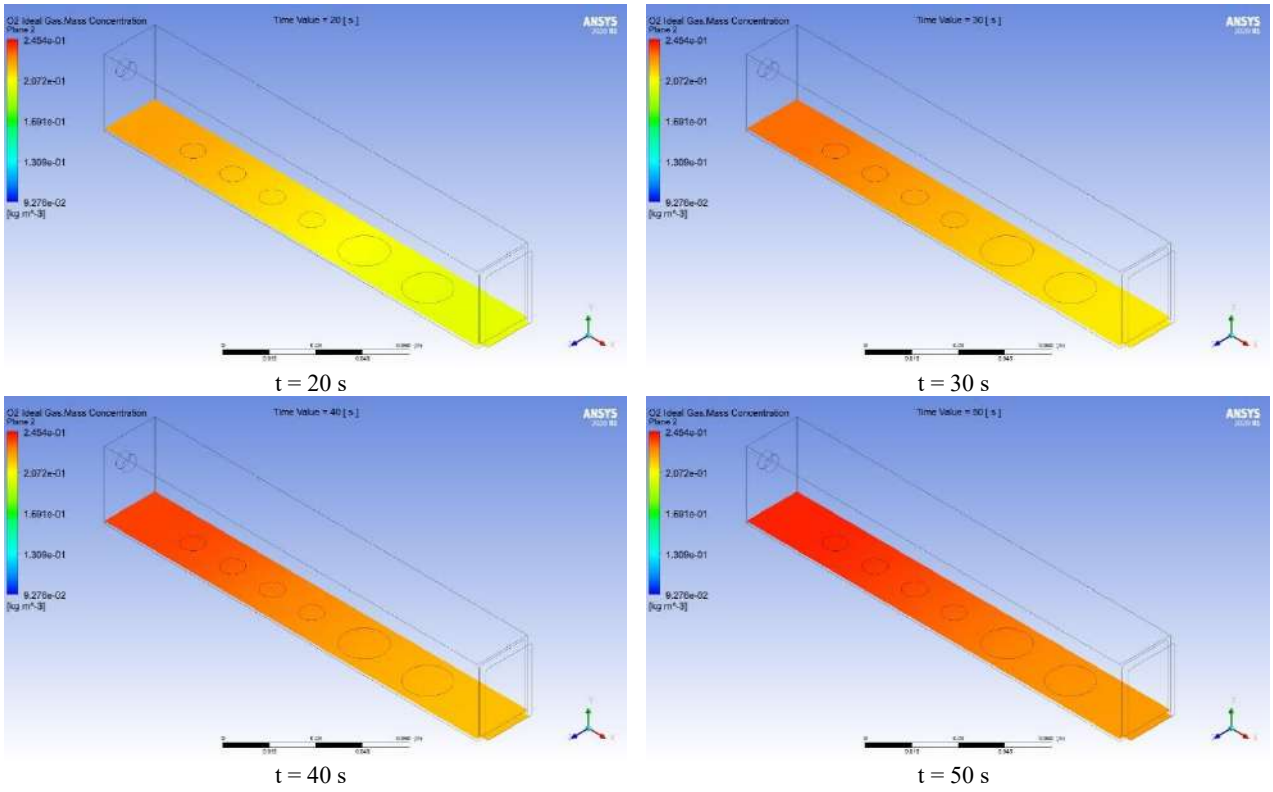

Figure 9 (continued) Simulation results variation of O_2 mass concentrations with time at plane XZ (y = 4 mm) for the laminar flow pattern.

The second flow simulation was created by a turbulent flow pattern with a gas flow rate of 0.4 liter per minute. The inlet airflow channel was an obstacle design for inducing turbulence and instigating turbulent flow. As shown in Figure 10, the airflow exhibited turbulent and swirling characteristics at the entrance. The turbulent flow was well-distributed throughout the cross-sectional area of the e-nose chamber. Additionally, the Reynolds number has been calculated within the e-nose chamber for testing this turbulent flow model, resulting in a Reynolds number of 2,374. When compared between the actual flow pattern (by smoke application) and the simulated model, it was found that the actual flow had a moderately dispersed swirling pattern and without a laminar behavior. Therefore, it could be concluded that the flow in this case was turbulent throughout the length of the e-nose chamber, as depicted in Figure 11.

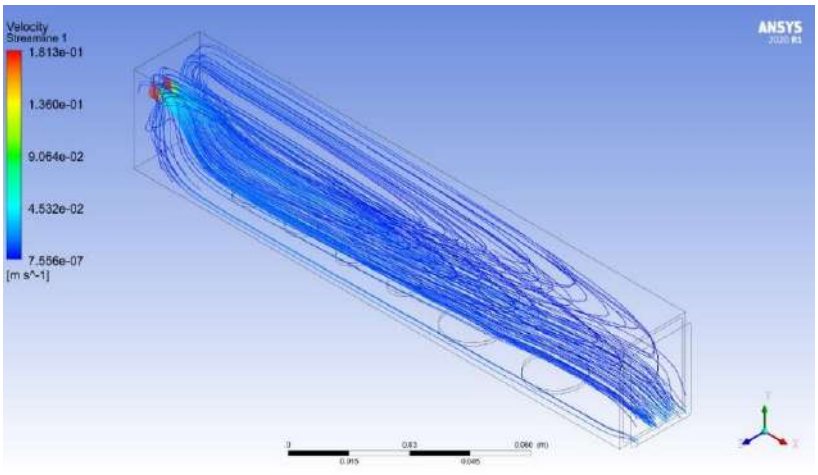

Figure 10 Gas flow model - turbulent flow.

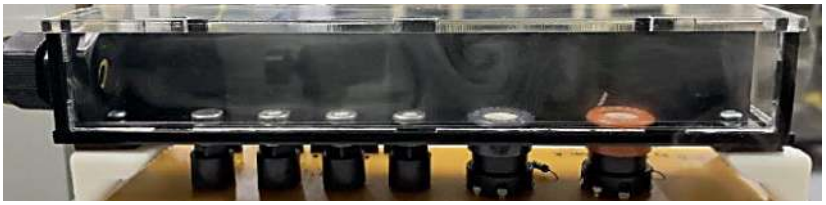

Figure 11 Smoke flow exhibits turbulent flow pattern.

The simulation results for the turbulent flow pattern of oxygen gas and oxygen mass concentration, with a high flow rate of 0.4 liters per minute at the inlet, are shown in Figures 12 and 13, respectively. In the simulation case, the flow velocity is relatively low, but it changes the flow cross-sectional area, leading to turbulent flow and resulting in a non-uniform flow of the gas sample. The velocity vector distribution does not change much with time, as seen in Figure 12. After 50 seconds, the final oxygen concentration field becomes almost uniform, exhibiting a distribution covering the entire gas sensor, as illustrated in Figure 13.

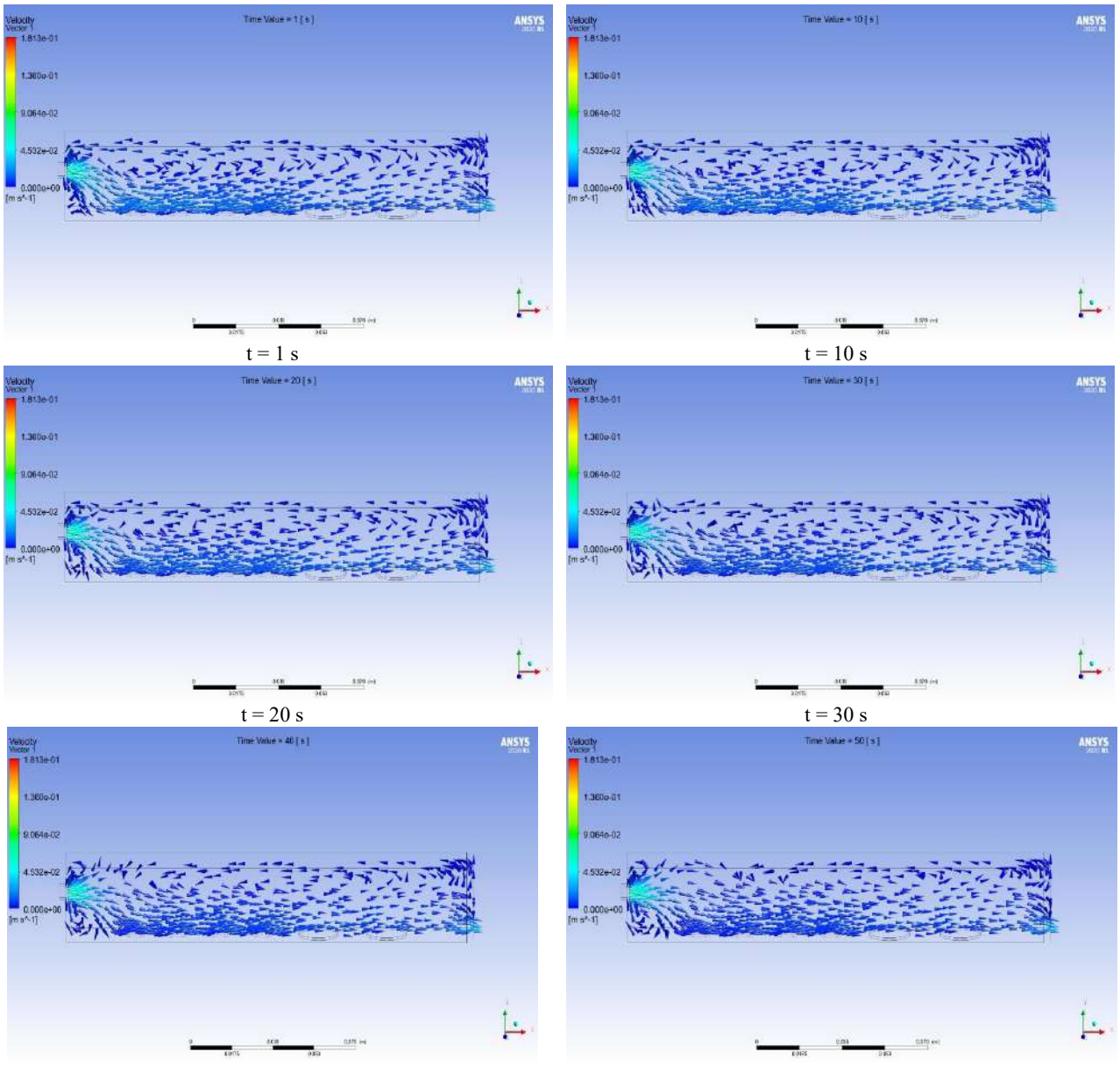

Figure 12 Simulation results on variation of O_2 velocity vector distribution with time at plane XY (z = 10 mm) for the turbulent flow pattern.

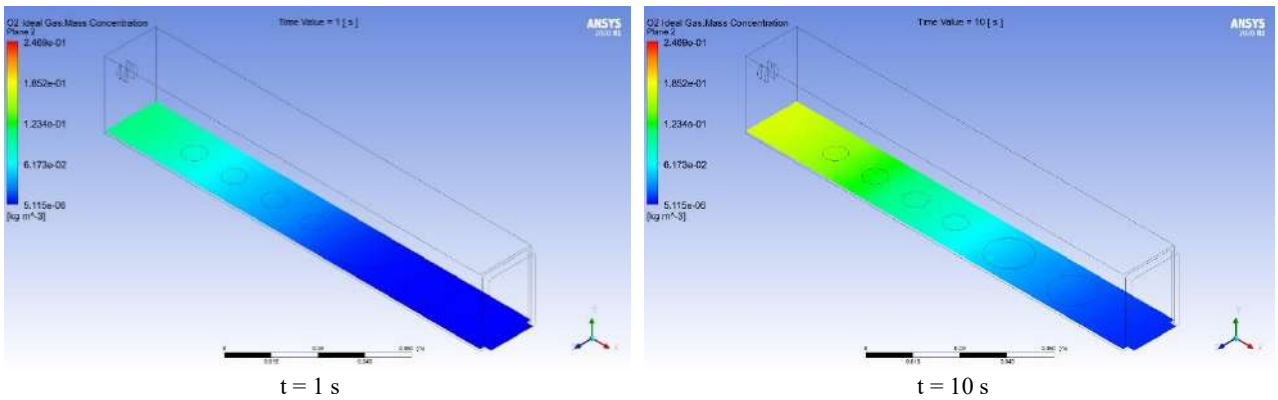

Figure 13 Simulation results variation of O_2 mass concentrations with time at plane XZ (y = 4 mm) for the turbulent flow pattern.

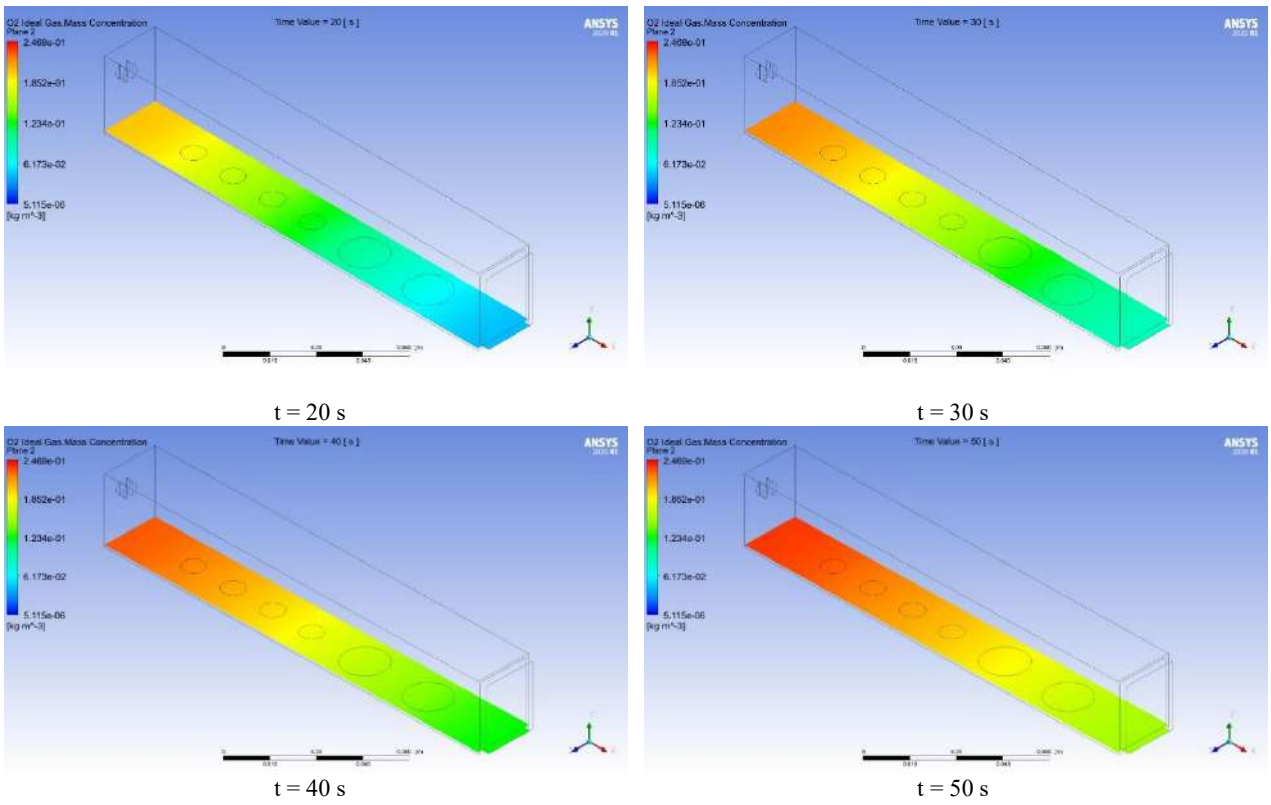

Figure 13 (continued) Simulation results variation of O_2 mass concentrations with time at plane XZ (y = 4 mm) for the turbulent flow pattern.

3.2 Results of testing rancid odor detection in brown rice with different gas flow patterns

E-nose tests with brown rice samples were conducted using laminar and turbulent flows. Raw data in the form of electrical potential difference signals were mathematically processed using the Savitzky-Golay smoothing method. The data points corresponding to high signal changes (transient state) were specifically selected for analysis, as shown in Figure 14.

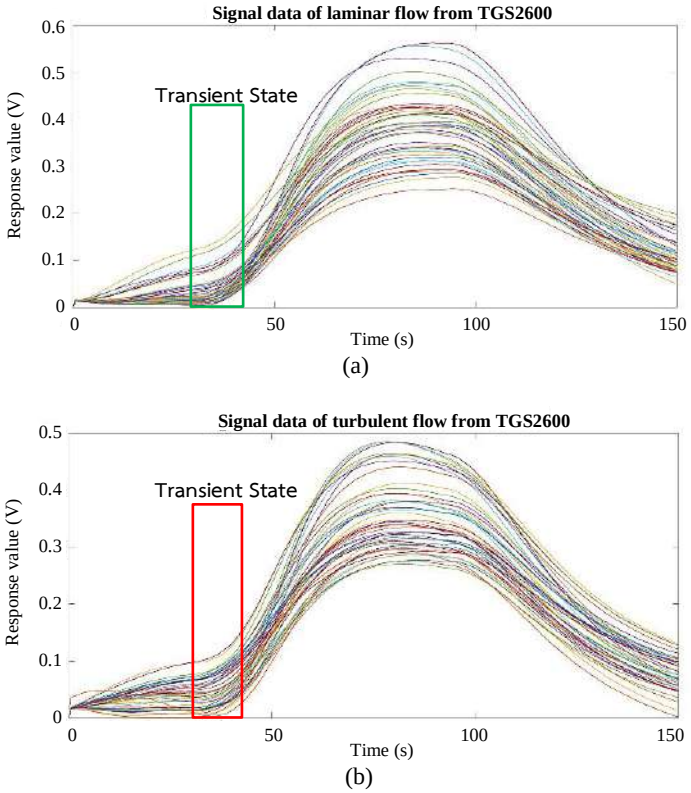

Figure 14 Data of the voltage difference signal from the TGS2600 gas sensor sample in (a) laminar flow and (b) turbulent flow.

The p-value, a statistical significance indicator, showed significant difference (P-value was very low) value which indicated high statistical significance, while a high p-value suggested low or no statistical significance. When analyzing signal data from the gas sensors, with each sensor providing 45 data points per airflow pattern, it was hypothesized that the slope or rate of signal change from a laminar flow would differ from that of a turbulent flow. The results showed that for five out of the six gas sensors (TGS2600, TGS2610, TGS2620, TGS813, and TGS822), their $p < 0.05$, which indicated a statistically significant difference in signal variation between the laminar and turbulent flow. Only the TGS2611 gas sensor revealed a p-value greater than 0.05, as shown in Table 3, indicating no significant rate of signal change. This could be attributed to its high specificity in detecting odors, which leads to a reduced response to the rancid odor of the brown rice sample. This assumption could be the cause of no significant difference between the two flow patterns. The summarized results are presented in Table 3.

Table 3 The average value of the signal data from the transient state.

Gas sensors	Average value (mV/sec)		P-value
	Laminar	Turbulent	
TGS-2600	7.389	6.626	0.014*
TGS-2610	9.733	7.958	0.000*
TGS-2611	2.122	2.110	0.888
TGS-2620	12.723	9.856	0.000*
TGS-813	5.137	3.708	0.000*
TGS-822	6.459	9.579	0.000*

[*] Means are significantly different from each other at $p < 0.05$.

Overall, it was concluded that the rate of signal change for gas sensors TGS2600, TGS2610, TGS2611, TGS2620, and TGS813 were higher in the laminar flow pattern compared to the other pattern. Moreover, using gas sensors in the e-nose system, a group of sensors is required to generate specific characteristics of the detected signals for odor discrimination. Study should further examine the relationship between the average rate of signal change during each transient state and the gas sensor.

4. Discussion

The analysis of the flow behavior through observation of the actual smoke compared to the flow patterns obtained from the CFD models of both laminar and turbulent flows was successful in confirming the expected flow patterns. However, it was noted that the smoke flow characteristics in the actual experimental setup exhibited differences in behavior or trajectories compared to certain aspects of the modeled patterns. This variation could be attributed to the influence of buoyancy forces [20], as suggested by the assumption that it might result from the influence of the buoyancy effect. This is due to the factors related to the density of the air inside the e-nose room, which is lower than the density of the smoke. Consequently, it indicates a downstream flow pattern of the smoke.

When considering the rate of change of the signal from the gas sensor that has the laminar flow, with the flow direction of the gas current perpendicular to the contact of the gas sensor corresponding to the work of [21, 22]. The flow laminar pattern allows the gas sample to contact evenly and consistently with the sensor, resulting in a favorable rate of signal change. This is based on similar research that discovered the laminar flow pattern was commonly used for odor testing due to its simplicity and ease of implementation [23, 24]. However, it is the case when similar turbulent flow techniques are tested. It was found to be effective in measuring [25, 26], but there was a slight difference in the direction of the parallel flow of the sample gas flow. This may be what allows the flow pattern to influence the response of the gas sensor. The result of the gas sensor at the final position in the e-nose gas chamber, showed the TGS822 gas sensor in the turbulent flow pattern provided a better rate of signal change when compared to the laminar flow pattern. This observation was made by analyzing the flow behavior of the laminar pattern along with the results. There was possibility that the gas sample flow might become slower or reverse in laminar pattern. Additionally, for the gas sensor placed at the final position in the e-nose chamber it was observed the appearance of air vortices when the air was pushed back. Moreover, such conditions are much more distant from the stable ones for the case without maintaining airflow. That can lead to increased noise and instability of measured results [27]. The utilization of the rancid odor from brown rice was used after the patterns of gas flow study using real smoke were done. The responses of these sensors were studied to compare real smoke and rancid odor. The wide range of rancid odors could be investigated in future work.

5. Conclusions

The developed airflow simulations are an efficient method to indicate a type of flow pattern. Laminar flow provided a better response from an array of sensors inside the e-nose chamber. The actual experiments of the e-nose using laminar and turbulent flow as a gas carrier to investigate the highest rate of signal voltage difference change resulted that the laminar flow pattern had five out of six gas sensors with higher average rate of change compared to turbulent flow patterns. This indicates that laminar-flow gas carrier provided better and rapid responsiveness for the array of gas sensors than turbulent flow. In the odor testing experiments using brown rice, at an airflow rate of 0.4 liters per minute, showed a positive trend for generating predictive equations for future outcomes.

6. Acknowledgments

The authors thank the Department of Mechanical Engineering, Chiang Mai University for providing facilities for fabricating and developing an e-nose device and thank Postharvest Technology Innovation Center, Office of the Higher Education Commission, Bangkok.

7. References

[1] Deshmukh S, Bandyopadhyay R, Bhattacharyya N, Pandey RA, Jana A. Application of electronic nose for industrial odors and gaseous emissions measurement and monitoring--an overview. Talanta. 2015;144:329-40.

[2] Gliszczyńska-Świgło A, Chmielewski J. Electronic nose as a tool for monitoring the authenticity of food. A review. Food Anal Methods. 2017;10(6):1800-16.
[3] Baietto M, Wilson AD. Electronic-Nose applications for fruit identification, ripeness and quality grading. Sensors (Basel). 2015;15(1):899-931.
[4] Karakaya D, Ulucan O, Turkan M. Electronic nose and its applications: a survey. Int J Autom Comput. 2020;17(2):179-209.
[5] Eusebio L, Capelli L, Sironi S. Electronic nose testing procedure for the definition of minimum performance requirements for environmental odor monitoring. Sensors. 2016;16(9):1548.
[6] Westenbrink E, Arasaradnam RP, O'Connell N, Bailey C, Nwokolo C, Bardhan KD, et al. Development and application of a new electronic nose instrument for the detection of colorectal cancer. Biosens Bioelectron. 2015;67:733-8.
[7] Taştan M, Gökozan H. Real-Time monitoring of indoor air quality with internet of things-based e-nose. Appl Sci. 2019;9(16):3435.
[8] Suchorab Z, Frac M, Guz L, Oszust K, Lagod G, Gryta A, et al. A method for early detection and identification of fungal contamination of building materials using e-nose. PLoS One. 2019;14(4):e0215179.
[9] Gobbi E, Falasconi M, Zambotti G, Sberveglieri V, Pulvirenti A, Sberveglieri G. Rapid diagnosis of Enterobacteriaceae in vegetable soups by a metal oxide sensor based electronic nose. Sens Actuators B Chem. 2015;207:1104-13.
[10] Loutfi A, Coradeschi S, Mani GK, Shankar P, Rayappan JBB. Electronic noses for food quality: a review. J Food Eng. 2015;144:103-11.
[11] Liang Z, Tian F, Zhang C, Sun H, Liu X, Yang SX. A correlated information removing based interference suppression technique in electronic nose for detection of bacteria. Anal Chim Acta. 2017;986:145-52.
[12] Pearce TC, Schiffman SS, Nagle HT, Gardner JW. Handbook of machine olfaction: electronic nose technology. Weinheim: Wiley; 2003.
[13] Neamsorn N, Changrue V, Kantakaew P, Promngam P. Electronic nose for classification of rancid odor in brown rice cv. Khao Dawk Mali 105. Agricultural Sci J. 2019;50(3):356-9. (In Thai)
[14] Zou X, Wang C, Luo M, Ren Q, Liu Y, Zhang S, et al. Design of electronic nose detection system for apple quality grading based on computational fluid dynamics simulation and k-nearest neighbor support vector machine. Sensors. 2022;22(8):2997.
[15] Loksupapaiboon K, Suvanjumrat C. Validation of wall functions for two-equation turbulence model of OpenFOAM. Eng J Res Dev. 2020;31(2):105-17. (In Thai)
[16] Launder BE, Spalding DB. The numerical computation of turbulent flows. Comput Methods Appl Mech Eng. 1974;3(2):269-89.
[17] Goody BA, Milton MJ. High-accuracy gas flow dilutor using mass flow controllers with binary weighted flows. Meas Sci Technol. 2002;13(7):1138.
[18] Zeng Y, Fang J. Numerical simulation and experimental study on gas mixing in a gas chamber for sensor evaluation. Meas: Sens. 2021;18:100338.
[19] Wang X, Qian C, Zhao Z, Li J, Jiao M. A novel gas recognition algorithm for gas sensor array combining Savitzky–Golay smooth and image conversion route. Chemosensors. 2023;11(2):96.
[20] Brahim K, Mourad B, Afif EC, Ali B. Control of smoke flow in a tunnel. J Appl Fluid Mech. 2013;6(1):49-60.
[21] Blixt Y, Borch E. Using an electronic nose for determining the spoilage of vacuum-packaged beef. Int J Food Microbiol. 1999;46(2):123-34.
[22] Kumar K, Rajput NS, Shvetsov AV, Saif A, Sahal R, Alsamhi SH. ID2S4FH: A novel framework of intelligent decision support system for fire hazards. Fire. 2023;6(7):248.
[23] Di Francesco F, Falcitelli M, Marano L, Pioggia G. A radially symmetric measurement chamber for electronic noses. Sens Actuators B: Chem. 2005;105(2):295-303.
[24] Kumar K, Rajput NS. Analysis space transformation based electronic nose for efficient detection and monitoring of volatile organic compounds, gases/odors in smart homes. Eur Chem Bull. 2023;12(Special Issue 7):513-28.
[25] Harmouzi M, Amari A, Masmoudi L. Conception and simulation of an electronic nose prototype for olfactory acquisition. Adv Sci Technol Eng Syst J. 2023;8(1):101-7.
[26] Chen Y, Xia W, Chen D, Zhang T, Song T, Zhao W, et al. A qualitative and quantitative analysis strategy for continuous turbulent gas mixture monitoring. Chemosensors. 2022;10(12):499.
[27] Borowik P, Grzywacz T, Tarakowski R, Tkaczyk M, Slusarski S, Dyshko V, et al. Development of a low-cost electronic nose with an open sensor chamber: application to detection of ciboria batschiana. Sensors. 2023;23(2):627.